Transactions of the Materials Research Society of Japan 28 [1] 97-104 (2003)

Sintering and Dielectric Characteristics of Tungsten Bronze Structured Ferroelectric $Sr_xBa_{1-x}Nb_2O_6$ Ceramics

Myoung-Sup Kim, Shin-Il Kang, Joon-Hyung Lee, Jeong-Joo Kim, Hee Young Lee* and Sang-Hee Cho**

Department of Inorganic Materials Engineering, Kyungpook National University, Daegu, 702-701, Korea

*Department of Materials Science and Engineering, Yeongnam University, Kyungsan, 712-749, Korea

**Fax: 82-53-950-5645, e-mail: shcho@knu.ac.kr

The tungsten bronze type of $Sr_xBa_{1-x}Nb_2O_6$(SBN) ($0.3 \leq x \leq 0.7$) ceramics was synthesized using the solid state reaction method. The mechanism of the abnormal grain growth in SBN ceramics was examined by using various experimental skills. The effect of Nb_2O_5 content on the microstructure evolution and dielectric characteristics was also examined. The relaxor behavior of the SBN ceramics as a function of the Sr/Ba ratio was quantitatively evaluated. Various situations in which the Sr and Ba cations occupy the A1 and A2 sites of the tungsten bronze structure were considered when the Sr/Ba ratio varied. A relationship between DPT behavior and ion ordering at A1 and A2 was analyzed theoretically. The experimental results are explained from the viewpoint of tungsten bronze crystallography of SBN ceramics.

Key words: Tungsten bronze structure, SBN, abnormal grain growth, DPT

1. INTRODUCTION

The tungsten bronze structure consists of a skeleton framework of MO_6 octahedra, sharing corners to form three different types of tunnels parallel to the c-axis in the unit cell formula of $[(A1)_2(A2)_4C_4][(B1)_2(B2)_8]O_{30}$.[1] As shown in Fig.1, both the 12-coordinated A1 site and 15-coordinated A2 site exist, corresponding to four-fold and five-fold tunnels, respectively. The 9-coordinated C-site has the smallest space among the three different types of tunnels created by the framework of octahedra.

Various tungsten bronze families exist.[2] One of the basic differences between tungsten bronzes can be attributed to A and/or C-site cation occupancy, which is determined by ionic valence, coordination number, and radius. Among the various tungsten bronze families, the empty bronzes have the A-site partially filled. This type is characterized by $Sr_{1-x}Ba_xNb_2O_6$ (SBN), which has a 5/6 occupancy (i.e. 1/6 vacancy) in the A-site and an empty C-site. Concerning ferroelectric $Sr_{1-x}Ba_xNb_2O_6$ ($0.25 \leq x \geq 0.75$; SBN) ceramics, which has a large pyroelectric[3-5] and linear electrooptic coefficients[1,6-8] as well as strong photorefractive effect,[9-11] the space of the A1 site is smaller than that of the A2 site. Therefore, it has been generally accepted that Sr occupies both A1 and A2 sites, but Ba was found only at the A2 site since the Sr ion radius is smaller than that of Ba.[12,13] In this case, when the ratio of Sr/Ba varies, the occupancy, distribution and ordering of Sr, Ba and vacancy at the A1 and A2 sites in the unit cell of tungsten bronze will change accordingly. This obviously will affect the dielectric characteristics of SBN ceramics.

Since SBN has superior optical properties and if someone wants to use it for an optical application, SBN ceramics should have near theoretical densities. However, considerable difficulties in sintering highly-dense SBN ceramics have been reported and abnormal grain growth(AGG) often occurs during sintering, which is assumed to be due to the formation of a liquid phase

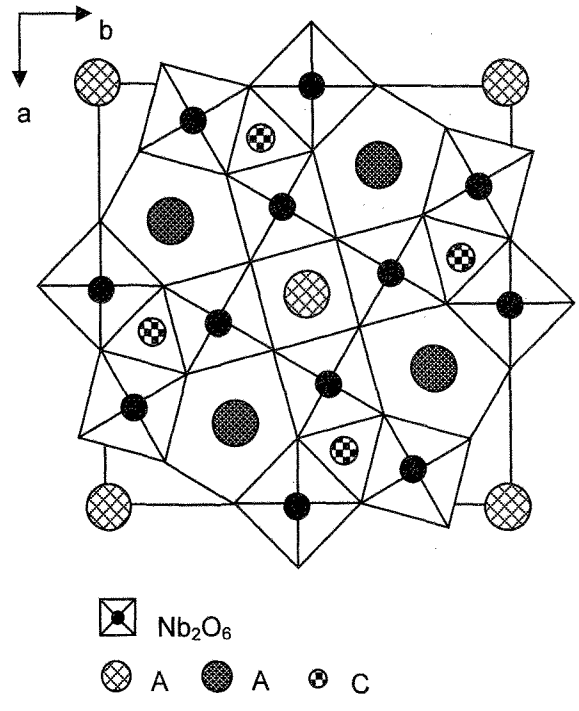

Fig.1 Atomic arrangement in a unit cell of a tungsten-bronze type structure projected along the c-axis (by P. B. Jamieson *et al.*[1]).

caused by local compositional deviation from stoichiometry.[14-18] Takahashi *et al.*[14] proposed that the small amount of liquid phase, which was formed due to an incomplete reaction during calcination is the reason of the AGG. Lee *et al.*[17,18] reported that the composition of the liquid phase at the grain boundary was Nb_2O_5-rich but BaO-deficient. However, a substantial mechanism to explain the formation of a liquid phase that results in AGG has not uncovered. On the other hand, Fang *et al.*[16] asserted that the $SrNb_2O_6$ (SN) second phase is decomposed from SBN during ball milling after calcinations. Thus, the second phase is the origin of the AGG. From this report, it is assumed that the indirect reason for the AGG in SBN ceramics is the SN phase. However, the liquid phase formation temperature of SN is over 1465℃, so there is no possibility of liquid phase formation during sintering. Moreover, even though the SN phase is formed as a second phase in SBN, SN has the same Nb/Sr cation ratio with that of SBN [Nb/(Sr+Ba)]. Thus the question of how the Nb-rich liquid phase could be generated emerges.

In this study, in order to examine the microstructural development behavior, diffusion couples between Nb_2O_5, $SrNb_2O_6$ (SN), $BaNb_2O_6$ (BN) and SBN ceramics were fabricated and sintered at different temperatures, and a more advanced mechanism of AGG in SBN ceramics is suggested. Dielectric characteristics were analyzed and compared with a theoretical calculation on the basis of cation distribution in the tungsten bronze structure. The effect of Nb_2O_5 content on the microstructure evolution and dielectric characteristics was also examined.

2. EXPERIMENTAL PROCEDURE

The starting materials of $Sr_xBa_{1-x}Nb_2O_6$ [x=0.3 (SBN30), 0.4(SBN40), 0.5(SBN50), 0.6(SBN60), 0.7(SBN70)], $SrNb_2O_6$ (SN) and $BaNb_2O_6$ (BN) were prepared from raw chemicals of $BaCO_3$(99.6%), $SrCO_3$(99.4%) and Nb_2O_5(99.9%) using the mixed oxide route. Different compositions of stoichiometric SBN70, x mol% Nb_2O_5-excess SBN70 and x mol% Nb_2O_5-deficient SBN70 were also prepared where x = 1, 3, 5. The compositions are denoted as SBN70 and SBN70±x hereafter. The weighed powders were wet mixed for 24 h in a plastic jar with zirconia balls and ethanol, then dried in an oven. The powders were calcined at 1300℃ for 6 h, then ball milled again for 24 h for crushing. 5wt% of aqueous PVA solution was mixed with the powders and sieved to form granules. Sintering was conducted at various temperatures for 2 h. Since the AGG frequently occurred when the samples were normally sintered, the dual-stage sintering method, which is known as an effective method of suppressing AGG in SBN ceramics,[17,18] was employed.

Shrinkage of samples during heating was measured using a vertical-loading dilatometer (Rigaku Thermoflex, TMA 8140). X-ray diffraction (XRD; Mac Science, M03XHF) studies were conducted on the sintered specimens to identify the phases. The densities of the sintered samples were measured using an immersion technique. For the microstructural observation of the samples, surfaces were polished and thermally etched. A scanning electron microscopy (SEM; JEOL, JSM-5400) was used for the microstructure observation. Grain sizes of sintered samples were determined using a linear intercept method.[19] For the dielectric measurements, Ag paste was screen-printed on both sides of the sample. Dielectric properties were analyzed by an impedance gain phase analyzer (HP4194A) with a frequency swept in steps from 1 kHz to 1 MHz as a function of temperature from -80 °C to 350°C in 2°C increment.

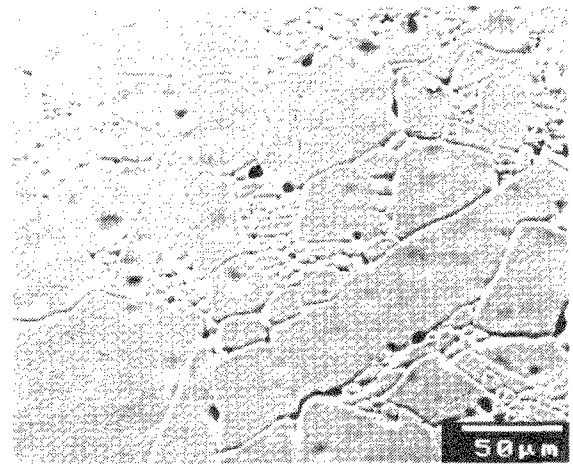

Fig.2 SEM photograph of SBN70 sample sintered at 1350℃ for 2 h.

3. RESULTS AND DISCUSSION

3.1 Mechanism of abnormal grain growth

Fig.2 shows the microstructure of the SBN70 sample sintered at 1350°C for 2 h. The duplex microstructure with a mixture of large abnormal grains and fine grains was developed in the sample. The origin of the AGG in

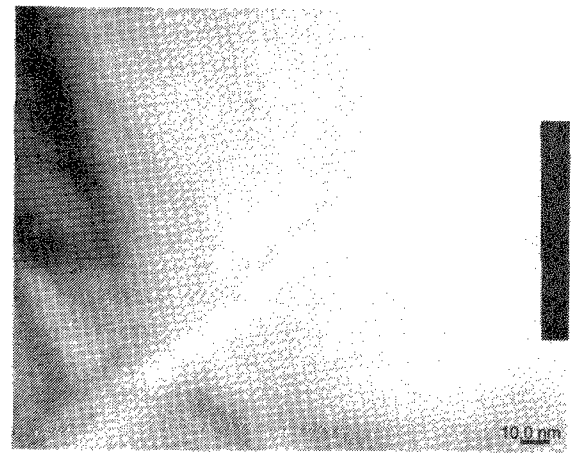

Fig.3 TEM photograph of SBN70 sample sintered at 1350℃ for 2 h.

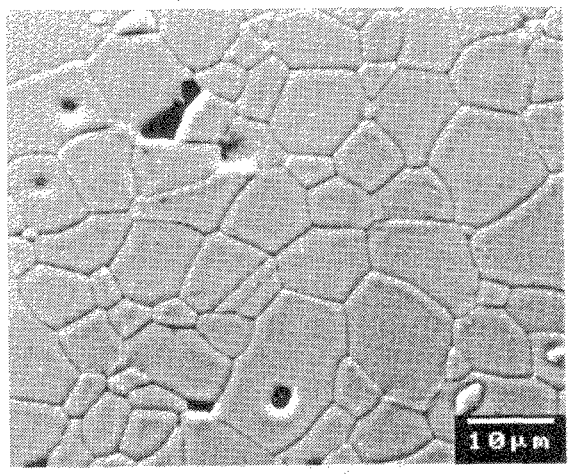

Fig.4 SEM photographs of SBN70 samples sintered at 1350℃ for 2 h after presintering at 1250℃ for 2 h.

stoichiometric SBN ceramics has been reported to be the inhomogeneous distribution of the Nb-rich liquid phase.[14-18]

Fig.3 shows a HRTEM micrograph of a grain boundary region of SBN70 which showed abnormal grain growth. Along the lattice fringes of grains, irregularly curved liquid film with a thickness about 6-8 nm was observed. This liquid phase seemed to be the Nb-rich liquid phase which is the reason of the AGG as proposed by Takahashi *et al.*[14] and Lee *et al.*[17,18]

When the sample is dual-stage sintered, as shown in Fig.4, a homogeneous microstructure without AGG was observed. The density of the sintered SBN70 sample showed 96.7±0.2%.

Fig.5 shows the microstructure of the SN-SBN50 diffusion couple that was sintered at 1300℃, 1350℃, 1400℃ for 2 h, respectively. In the case of the sample in Fig.5(a), which was sintered at 1300℃, the SN above was composed of fine grains with sizes below 5㎛. On the other hand, SBN50 below was composed of grains with sizes about 10㎛. AGG was not found in either case. In the case of the sample in Fig.5(b), which was sintered at 1350℃, no difference in grain size was found at the interface or the inner part of SN. While SBN50 was composed of about 20㎛ grains, the initiation of AGG over 50㎛ was seen at the interface. In the case of the sample in Fig.5(c), which was sintered at 1400℃, a number of cracks and no difference in grain size at the interface or inner part of SN were seen, similar to the case of the sample in Fig.5(b). However, abnormal grains hundreds of micrometers in size were observed at the interface of SBN50. It is generally accepted that the presence of large grains is responsible for the formation of cracks because cracking begins when grain size exceeds a critical value.[20,21] Furthermore, large internal stresses are induced in the sample when the sample passes the phase transformation temperature during cooling after sintering. The generation of cracks also

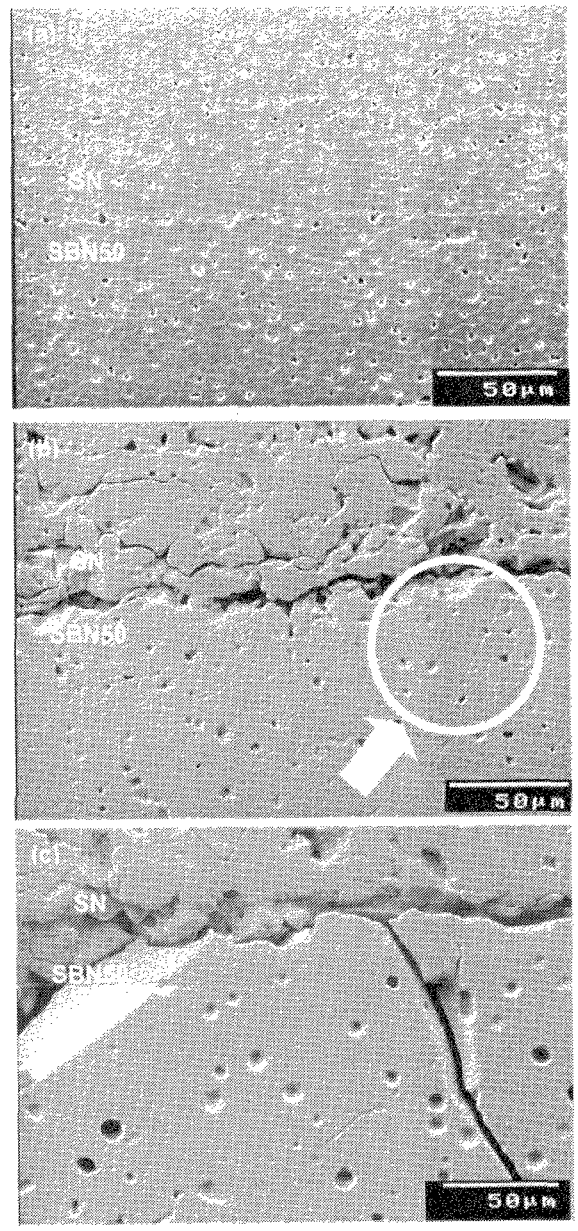

Fig.5. SEM photographs of the SBN50-SN diffusion couple sintered at (a) 1300℃ (b) 1350℃ and (c) 1400℃ for 2 h after presintering at 1250℃ for 4 h. Arrow indicates the initiation of AGG.

seems to attributed to the internal stresses.

Fig.6 shows the microstructure of SN-SBN30 and SN-SBN70 diffusion couples sintered at 1400℃ for 4 h. AGG was observed regardless of the Sr/Ba ratio, at the interfaces stretching down to the SBN section in both diffusion couples. This result coincides with the reports by Takahashi and Fang[14,16] that the SN is the source of the AGG. Notice that the diffusion couples were sintered at 1400°C, which is lower than the melting temperature of the SN phase.

In the case of BN-SBN50 diffusion couple, even the microstructures are not presented, the AGG development behavior showed the same tendency with the SN-SBN50 diffusion couple. From this result, we found that AGG

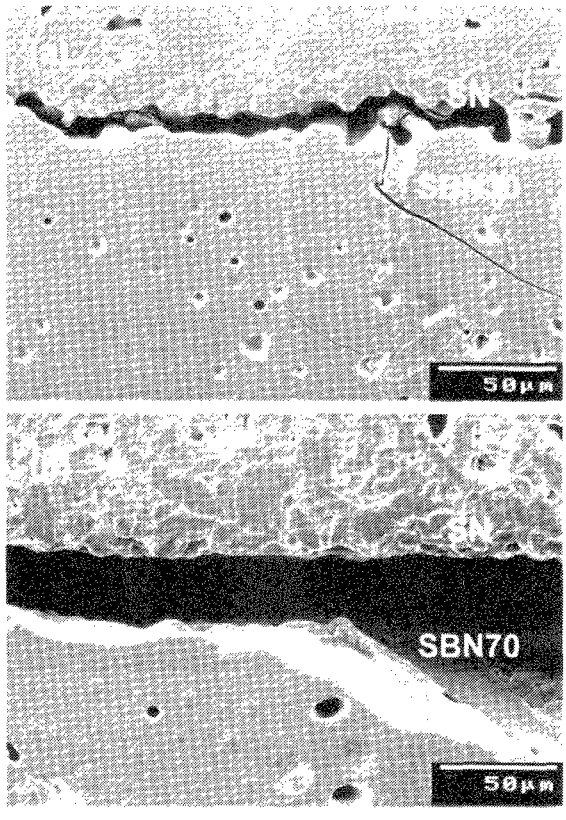

Fig.6. SEM photographs of the (a) SBN30-SN and (b) SBN70-SN diffusion couples sintered at 1400℃ for 2 h after presintering at 1250℃ for 4 h.

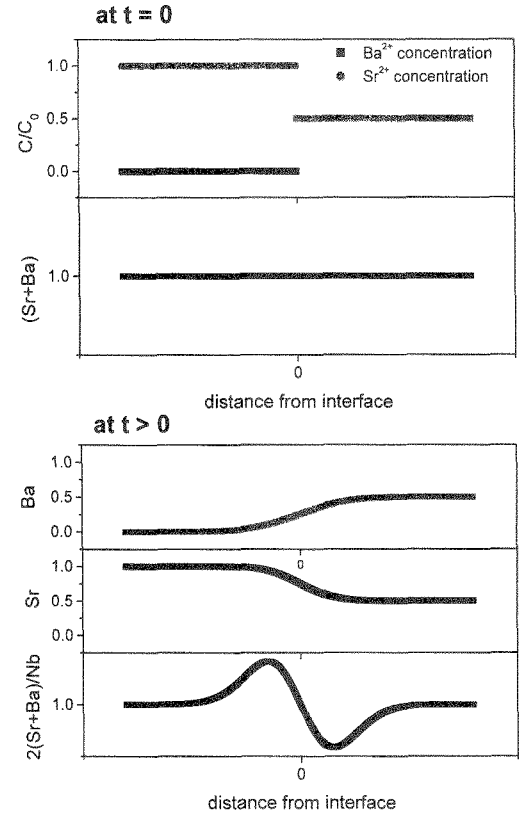

Fig.7. Theoretical calculation of concentration gradient of Ba and Sr ions near the SN and SBN50 interface (Assumtion: $D_{Sr} < D_{Ba}$).

emerged in SBN whether the diffusion couple faced the SN or BN. However, it is hard to imagine that the SN and BN phases melted at 1400°C because they have much higher melting points of 1465°C and 1435°C, respectively. According to the SBN phase diagram,[22] we can select a candidate phase of Nb-rich $Ba_3Nb_{10}O_{28}(B_3N_5)$ s.s. as a liquid former at 1350°C, which is the temperature that the AGG seed formed in Fig.5(b). Therefore, we can imagine that the $Ba_3Nb_{10}O_{28}$ phase was created somehow during sintering.

When two samples of unequal composition are brought into intimate contact across a plane interface, interdiffusion is allowed to occur under the condition that the concentration at the surface is maintained at a constant during the whole process, and specific surface concentration C_0 at time zero being exposed to a constant activity source of diffusant. For diffusion through a plane surface normal to the direction, the concentration change with respect to distance x and time t at the interface between A and B can be depicted as follows:[23]

$$c(x,t) = c_{A_0} + \frac{c_{B_0} - c_{A_0}}{2}\left[1 - erf\left(\frac{x}{2\sqrt{Dt}}\right)\right] \quad (1)$$

where $c(x,t)$ is the concentration with respect to x and t, C_{A0} is the initial concentration of A, C_{B0} is the initial concentration of B, D is the diffusion coefficient, x is the distance from the interface and t is time. For instance, when the SN-SBN50 diffusion couple is applied to equation (1), let the Sr concentration of SN be 1, the Ba concentration of SN be 0, the Sr concentration of SBN be 0.5, and the Ba concentration of SBN be 0.5. At the initial stage of diffusion, the concentration of Sr and Ba forms a step function at the interface. However, the overall concentration ratio of 2(Sr+Ba)/Nb is identical on both sides as Fig.7(a) shows. With the passage of time, however, after the diffusion of ions has proceeded under the condition $D_{Ba} > D_{Sr}$, the result of a computer simulation shows that the concentration gradient of each ion at the interface appears. This inevitably results in an unbalanced concentration ratio of 2(Sr+Ba)/Nb, as depicted in Fig.7(b). If the diffusion coefficient of D_{Ba} is smaller than D_{Sr}, the areas of which the concentration 2(Ba+Sr)/Nb is smaller or larger than 1 also develop on both sides of the interface. On the other hand, since the Nb concentration is equal in SN and SBN, steady state diffusion of Nb is assumed to occur. Consequently, when the diffusion coefficients of Sr and Ba differ, the area with a high 2(Sr+Ba)/Nb concentration could be defined as a Nb-deficient area, while the area with a low 2(Sr+Ba)/Nb concentration could be defined as a Nb-rich area. In the Nb-rich area, the $Ba_3Nb_{10}O_{28}$ s.s. phase is believed to be produced. When the $Ba_3Nb_{10}O_{28}$ s.s. phase produces a liquid phase during sintering it might be

(Received December 21, 2002; Accepted January 31, 2003)

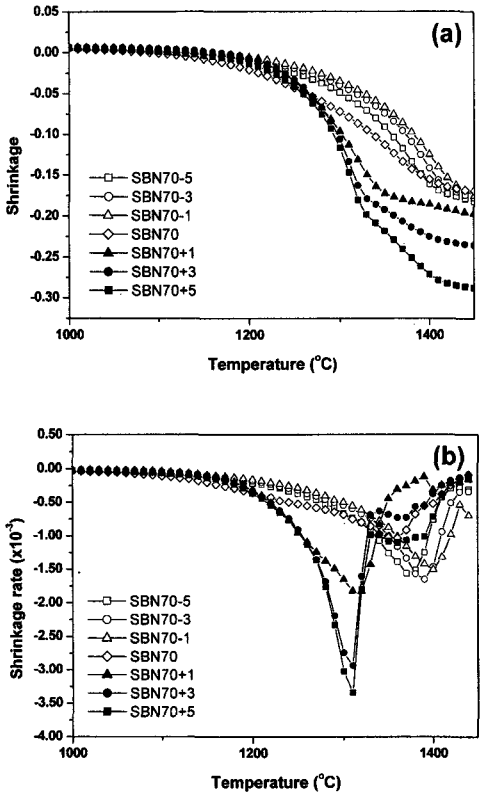

Fig.8 Densification behavior of samples: (a) shrinkage and (b) shrinkage rate

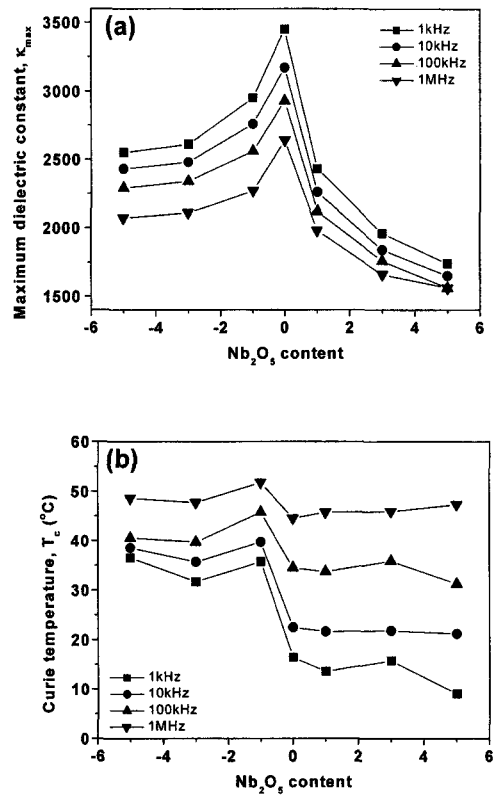

Fig.9 Variations of (a) maximum dielectric constant and (b) the Curie temperature of samples sintered at 1350℃ for 2h as function of Nb_2O_5 content and frequency

inhomogeneously distributed in the sample, which eventually results in AGG. Consequently, due to the difference between the diffusion coefficients of Sr and Ba, the generation of a Nb-rich area occurs in both the SN-SBN and BN-SBN diffusion couples. This signifies that AGG could be generated in SBN samples regardless of the Sr/Ba ratio when the SN or BN phase is produced as a second or intermediate phase in SBN during sintering. Based on this result, we can predict the production of Nb-rich areas at interfaces where two different kinds of SBN powder with different Sr/Ba ratios are mixed with each other, not only in the SN-SBN and BN-SBN diffusion couple cases.

3.2 Effect of Nb_2O_5 content

Fig.8 shows the densification behavior of shrinkage and the shrinkage rate of the samples as a function of Nb_2O_5 content. The densification behavior of the samples was clearly influenced by the Nb_2O_5 content. Most of the densification for the stoichiometric and Nb_2O_5-deficient samples occurred in the high sintering temperature range of 1360-1400°C. A small amount of excess Nb_2O_5 significantly enhanced densification at the relatively low sintering temperature of 1320°C; another shrinkage peak around 1370°C was also observed. The first shrinkage around 1320°C is believed to have been due to a liquid phase, which accelerates densification at low temperatures. Another peak in densification at around 1370°C also occurred between solid grains as observed in the stoichiometric and Nb_2O_5-deficient samples. The phase diagram[22] of SBN ceramics also supports the formation of a liquid phase above 1320°C.

According to the x-ray analysis, traces of second phases $Sr_2Nb_2O_7$ s.s. (S_2N) and $Ba_3Nb_{10}O_{28}$ s.s. (B_3N_5) in 5 mol% Nb_2O_5-deficient and 5 mol% Nb_2O_5-excess samples are appeared, respectively. On the basis of the phase diagram,[22] S_2N has a eutectic temperature of >1420°C, while that of the B_3N_5 phase is around 1320°C. Therefore, when the Nb_2O_5-excess sample is sintered around or over 1320°C, the second phase of B_3N_5 will form a liquid phase, which seems to play a major role in abnormal grain growth in the system.

Fig.9(a) shows the maximum dielectric constant of the samples sintered at 1350°C for 2 h as functions of Nb_2O_5 content and measurement frequency. The maximum dielectric constants show the highest value at the stoichiometry composition and decreased as the composition went away from the stoichiometry. This is believed to be due to the second phases in the matrix. Because the dielectric constant of the $Sr_2Nb_2O_7$ is below 100 at the temperature range measured,[24] the second phase of $Sr_2Nb_2O_7$ s.s. seems to have a lower dielectric

constant than the ferroelectric matrix. Even a specific dielectric constant of the $Ba_3Nb_{10}O_{28}$ s.s. phase could not present here, though, the decreased dielectric constant in the Nb_2O_5-excess sample implies that the $Ba_3Nb_{10}O_{28}$ s.s. phase has a lower dielectric constant than the matrix. Based on this assumption, because the second phase of B_3N_5 forms a liquid phase during sintering due to its low melting point, the non-ferroelectric liquid phase at the grain boundaries surrounds the ferroelectric grains even though the microstructure in not shown here. Therefore, the dielectric constant degraded more in the Nb_2O_5-excess samples than in the Nb_2O_5-deficient samples in which the second phase of S_2N solid grains are scattered in the matrix. Fig.9(b) shows the Curie temperatures of the samples derived from dielectric constant curves as functions of Nb_2O_5 content and measurement frequency. The dielectric characteristics show diffuse phase transition (DPT) phenomena (i.e., they exhibit a broad Curie temperature range with respect to the frequency). Note that the Curie temperatures of the samples in Nb_2O_5-deficient area are higher than in the Nb_2O_5-excess area. The shift of the Curie temperatures implies a change in the Sr/Ba ratio of the matrix. Hence, it is necessary to confirm the composition change of the matrix due to the formation of second phases. The second phase of B_3N_5 formed in the Nb_2O_5-excess area that contains Ba, while the second phase of S_2N formed in the Nb_2O_5-deficient area that contains Sr. This naturally affects the Sr/Ba ratio of the matrix, which is directly connected to the Curie temperature; in other words, the lower the Sr/Ba ratio, the higher the Curie temperature.[3,8] The difference of the Curie temperature (ΔT_c) at different frequencies, for example 1 kHz and 1 MHz, indicates the frequency dependence of the Curie temperature.[25] According to the measured data in Fig. 9(b), ΔT_c for the Nb_2O_5-deficient, stoichiometry and Nb_2O_5-excess compositions show 12, 28 and 38 °C, respectively, which suggests that the Nb_2O_5-excess sample shows more diffused phase transition. It is reported that the degree of DPT increases when the Sr/Ba ratio increased.[3,8,26] From this point of view, therefore, the greater DPT phenomena in the Nb_2O_5 excess composition probably reflects the formation of a $Ba_3Nb_{10}O_{28}$ second phase, which increased the Sr/Ba ratio of the matrix. On the other hand, the connectivity between the ferroelectric and non-ferroelectric phases in a sample composed of ferroelectric and non-ferroelectric mixtures might play a role in dielectric behavior.[27]

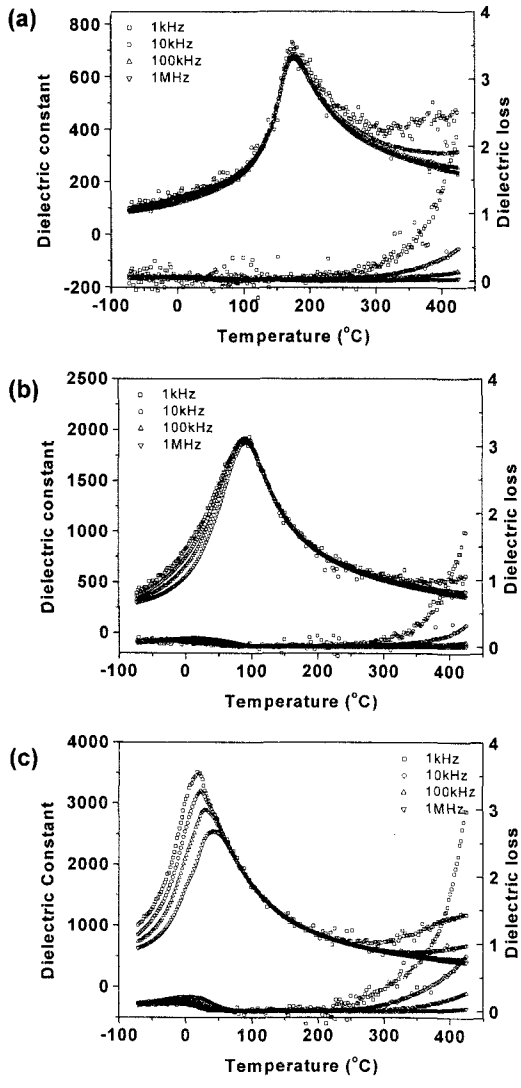

Fig.10 Temperature dependence of dielectric constant and dielectric loss of (a) SBN30 (b) SBN50 and (c) SBN70 samples measured at different frequencies.

3.3 Cation distribution and dielectric behavior

Fig.10 exhibits the dielectric constant of the sintered samples as functions of frequency and temperature. The phase transformation temperature decreases while the maximum dielectric constant increases as the Sr/Ba ratio increases.

In order to evaluate the quantified degree of DPT behavior of the SBN samples, following equations were used.[28]

$$\frac{1}{\kappa} - \frac{1}{\kappa_{max}} = \frac{(T - T_C)^\gamma}{C} \quad (1)$$

$$\frac{\kappa_{max}}{\kappa} = 1 + \frac{\kappa_{max}}{C}(T - T_C)^\gamma \quad (2)$$

where κ is the dielectric constant, κ_{max} is the maximum dielectric constant, T is the temperature, T_C is the phase transformation temperature, γ is the diffuseness coefficient, and C is the Curie-like constant. From the equations, the γ and C/κ_{max} values can be obtained.

The γ and C/κ_{max} values with respect to the Sr/Ba ratio are summarized in Fig.11. A high correlation of the γ value with the plane transformation diffuseness was found.[25,28] In the case of $BaTiO_3$ revealing a typical sharp phase transformation, which follows the Curie-

(Received December 21, 2002; Accepted January 31, 2003)

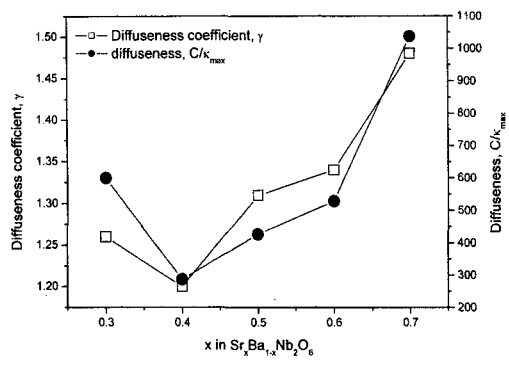

Fig.11 Variation of the diffuseness coefficient (γ) and diffuseness (C/κ_{max}) of samples as a function of Sr content.

Weiss law, has a γ value nearly equal to 1. Whereas the γ value is as large as 1.7 for the materials with a very diffused transformation like PMN and PZN. Therefore, γ is accepted empirically as representing a first-order phase transformation when it is 1 and a second-order phase transformation when it is 2.[25] On the other hand, C/κ_{max} represents the measure of the diffuseness, as the fall-off rate of κ/κ_{max}. In Fig.11, γ exhibited its lowest value at SBN40, but increased when the Sr content went further from SBN40. C/κ_{max} also marked its lowest value at SBN40. This signifies that SBN40 approaches first-order phase transformation. The degree of DPT decreases as well. The degree of DPT in SBN ceramics with respect to the Sr/Ba ratio can be explained by the degree of disorder of Sr and Ba ions in the A1 and A2 sites, because the degree of disorder is directly related with the DPT behavior.[29,30] From this point of view, we can predict the DPT behavior of various supposed occupation conditions by evaluating the degree of disorder of each condition.

In SBN ceramics, occupation condition of vacancy, Sr, and Ba in the A1 and A2 sites at different Sr/Ba ratios can be considered. On the basis of tungsten bronze structure, we can assume that the one vacancy out of six is put into the A1 or A2 sites by desired ratio. Then, the other five out of six sites are filled with Sr and Ba ions according to the Sr/Ba ratio. In this case, preferred sites should be considered, that is, Ba should go to the A2 site, Sr to the A1 site and the rest of the ions fill the remaining sites. When we summarize this simple calculations, we can evaluate the degree of disorder of each site from the occupation ratio and find out where the vacancy prefers to go as a function of Sr/Ba ratio.

The degree of disorder can be expressed by the Boltzmann equation, which was designed to evaluate lattice entropy. In case of a large degree of disorder, we can anticipate that lattice entropy increases when the degree of DPT increases.

$$S = k\ln W = k\ln(W_{A1}\times W_{A2}) = k(\ln W_{A1} + \ln W_{A2}) \quad (3)$$

S is the entropy of the system, k is the Boltzmann constant, and W, W_{A1} and W_{A2} are the number of ways of distributions of the total A site, A1 site and A2 site, respectively. W_{A1} and W_{A2} can be expressed theoretically as:

$$W_{A1} = \frac{(Ba_{A1} + Sr_{A1} + V_{A1})!}{Ba_{A1}!\times Sr_{A1}!\times V_{A1}!} \quad (4)$$

$$W_{A2} = \frac{(Ba_{A2} + Sr_{A2} + V_{A2})!}{Ba_{A2}!\times Sr_{A2}!\times V_{A2}!} \quad (5)$$

Ba_{A1}, Sr_{A1} and V_{A1} represent the number of Ba, Sr and vacancy in the A1 site, while Ba_{A2}, Sr_{A2} and V_{A2} represent the number of Ba, Sr and vacancy in the A2 site. When equations (4) and (5) are substituted into equation (6),

$$S = k\left[\ln\frac{(Ba_{A1} + Sr_{A1} + V_{A1})!}{Ba_{A1}!\times Sr_{A1}!\times V_{A1}!} + \ln\frac{(Ba_{A2} + Sr_{A2} + V_{A2})!}{Ba_{A2}!\times Sr_{A2}!\times V_{A2}!}\right] \quad (6)$$

Stirling's approximation is expressed by,

$$\ln N! \approx N\ln N - N \quad (7)$$

Using the approximation, the equation (6) can be expressed as,

$$S = k\left[\begin{array}{l}\left\{(Ba_{A1} + Sr_{A1} + V_{A1})\ln(Ba_{A1} + Sr_{A1} + V_{A1})\right. \\ \left.-Ba_{A1}\ln Ba_{A1} - Sr_{A1}\ln Sr_{A1} - V_{A1}\ln V_{A1}\right\} \\ +\left\{(Ba_{A2} + Sr_{A2} + V_{A2})\ln(Ba_{A2} + Sr_{A2} + V_{A2})\right. \\ \left.-Ba_{A2}\ln Ba_{A2} - Sr_{A2}\ln Sr_{A2} - V_{A2}\ln V_{A2}\right\}\end{array}\right] \quad (8)$$

The entropy can be calculated by the Ba/Sr ratio and it depends on the occupation ratio of the vacancies existing in the A1 and A2 sites.

Fig.12 shows the number of ways of distributions of the total A sites with respect to the vacancy occupation ratio in the A1 and A2 sites. The number of ways of distributions was calculated for 1000 unit cells. When a vacancy exists only in the A2 site, the number of distributions marked the minimum value at x=0.4, but increased when x went further from 0.4. This tendency shows a similarity with Fig.11, which depicts DPT

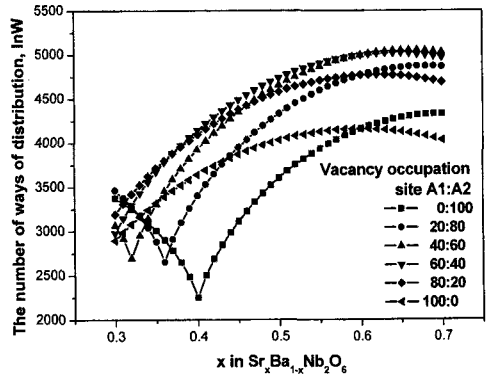

Fig.12 The number of ways of distributions as functions of the Sr/Ba ratio and vacancy occupation.

behavior. When the vacancy amount increases in the A1 site, the entropy minimum shifts to x=0.3 when 60 % of the vacancy occupies A1 sites. Consequently, it is concluded that the vacancy prefers the A2 site to the A1 site. Even though a detailed method and results are not discussed here, we did calculate the electrostatic potentials of each ionic site using an unpublished computer program.[30,31] In the case when the vacancy occupies the A2 site, the lattice energy was lower than the case when the vacancy occupies the A1 site. This implies that the vacancy at the A2 site is electrostatically preferred, which makes the lattice stable electrostatically. This result of vacancy preference agrees with the other literature published, which reported on the ion occupancy at each site by x-ray measurement and crystal structure analysis.[1,2]

4. CONCLUSION

Concerning the AGG in SBN, interdiffusion occurs due to the concentration gradient when the second or intermediate phase is produced during synthesis and/or sintering. Because of the difference between the diffusion coefficients of Sr and Ba, a Nb-rich area develops at the interface between the second phase and the matrix, which produces Nb-rich liquid phase and behaves as the origin of AGG. Second phases of $Ba_3Nb_{10}O_{28}$ and $Sr_2Nb_2O_7$ were found in the Nb_2O_5-excess and Nb_2O_5-deficient samples, respectively. The second phases of $Ba_3Nb_{10}O_{28}$ and $Sr_2Nb_2O_7$ changed the Sr/Ba ratio of the matrix. It was found that the Curie temperature shifted and the dielectric constants, as well as DPT behavior, were influenced accordingly. For a quantitative evaluation of DPT behavior of SBN ceramics, γ and C/κ_{max} were calculated. The weakest DPT behavior was observed in SBN40. An increased DPT is correlated to the increase in the number of ways of distributions by disordered occupation of Sr, Ba and vacancy in the A1 and A2 sites. When we calculated the number of ways of distributions according to the vacancy occupation ratio in the A1 and A2 sites, the number of ways was lowest when the vacancy occupies the A2 sites. This coincides with the lowest DPT behavior of SBN40.

ACKNOWLEDGEMENTS

This work was supported by Grant No. R01-2000-000-00233-0 from the Basic Research Program of the Korea Science & Engineering Foundation.

REFERENCES

1. P. B. Jamieson, S. C. Abrahams and J. L. Bernstein, *J. Chem. Phys.*, **48,** 5048-57 (1968).
2. Yuhuan Xu, "Ferroelectric Materials and Their Applications", Elsevier Science Publishers, (1991) pp.247-276.
3. A. M. Glass, *J. Appl. Phys.*, **40,** 4699-713 (1969).
4. S. I. Lee and W. K. Choo, *Ferroelectrics*, **87,** 209-12 (1988).
5. A. M. Glass, *Appl. Phys. Lett.*, **13,** 147-9 (1968).
6. P. V. Lenzo, E. G. Spencer and A. A. Ballman, *Appl. Phys. Lett.*, **11,** 23-4 (1967).
7. K. Nagata, Y. Yamamoto, H. Igarashi and K. Okazaki, *Ferroelectrics*, **38,** 853-6.
8. N. S. VanDamme, A. E. Sutherland, L. Jones, K. Bridger and S. R. Winzer, *J. Am. Ceram. Soc.*, **74,** 1785-92 (1991).
9. T. Imai, S. Yagi, K. Yamazaki and M. Ono, *Jpn. J. Appl. Phys.*, **38,** 1984-1988 (1999).
10. E. L. Venturini, E. G. Spencer, P. V. Lenzo and A. A. Ballman, *J. Appl. Phys.*, **39,** 343-4 (1968).
11. M. D. Ewbank, R. R. Neugaonkar, W. K. Cory and J. Feinberg, *J. Appl. Phys.*, **62,** 374-80 (1987).
12. W. H. Huang, Z. Xu and D. Viehland, *Philosophical Magazine A*, **71,** 219-29 (1995).
13. R. Guo, A. S. Bhalla, G. Burns and F. H. Dacol, *Ferroelectrics*, **93,** 397-405 (1989).
14. J. Takahashi, S. Nishiwaki and K. Kodaira, *Ceram. Trans.*, **41,** 363-370 (1994).
15. S. Nishiwaki, J. Takahashi and K. Kodaira, *Jpn. J. Appl. Phys.*, **33,** 5477-81 (1994).
16. T. T. Fang, E. Chen and W. J. Lee, *J. Euro. Ceram. Soc.*, **20,** 527-30 (2000).
17. H. Y. Lee and R. Freer, *J. Appl. Phys.*, **81,** 376-82 (1997).
18. H.Y. Lee and R. Freer, *J. Mater. Sci.* **33,** 1703-8 (1998).
19. R. L. Fullmann, *Trans. AIME*, **3** 447 (1953).
20. J. A. Kuszyk and R. C. Bradt, *J. Am. Ceram. Soc.*, **56,** 420 (1973).
21. J. J. Cleveland and R. C. Bradt, *J. Am. Ceram. Soc.*, **61,** 478 (1978).
22. J. R. Carruthers and M. Grasso, *J. Electrochem. Soc.*, **117,** 1426-30 (1970).
23. P. Shewmon, "Diffusion in Solids, The Minerals, Metals & Materials Society", Pennsylvania, 1989, 2nd ed., Ch.1, p. 22.
24. O. Madelung, "Landolt-Börnstein, Vol.28: Ferroelectric and Related Substances", Fig. 619, Springer-Verlag, Berlin, 1990.
25. S. J. Butcher and N. W. Thomas, *J. Phys. Chem. Solids*, **52,** 595-601 (1991).
26. D. Viehland, Z. Xu, and W. H. Huang, *Philosophical Magazine A*, **71,** 205-17 (1995).
27. J. H. Sohn, J. W. Cho, J. H. Lee, and S. H. Cho, *Solid State Ionics*, **108,** 141-9 (1998).
28. K. Uchino and S. Nomura, *Ferroelectric Lett.*, **44,** 55 (1982).
29. L. E. Cross, *Ferroelectrics*, **76,** 241-67 (1987).
30. L. E. Cross, *Ferroelectrics*, **151,** 305-20 (1994).
31. Program MADEL, coded by K. Kato, NIRIM, Japan.
32. Y. Kanke, *Phys. Rev B.* **60,** 3764 (1999).